JOURNAL OF SPACECRAFT AND ROCKETS
Vol. 45, No. 6, November–December 2008

Analysis of an Electromagnetic Mitigation Scheme for Reentry Telemetry Through Plasma

Minkwan Kim*
University of Michigan, Ann Arbor, Michigan 48109
Michael Keidar†
George Washington University, Washington, D.C., 20052
and
Iain D. Boyd‡
University of Michigan, Ann Arbor, Michigan 48109

DOI: 10.2514/1.37395

During hypersonic reentry flight, the shock heated air generates a weakly ionized plasma layer. Because the weakly ionized plasma layer has a high plasma number density, it causes an important systems operation problem that is known as a communication, or radio, blackout. The radio blackout occurs when the plasma frequency of the plasma layer is higher than a radio wave frequency. In this case, the radio wave signals to and from the vehicle are reflected or attenuated so that the vehicle loses voice communication, data telemetry, and Global Positioning System navigation. The radio blackout problem can be solved by reducing the plasma number density of the plasma layer because the plasma frequency is mainly related to the plasma number density of the plasma layer. To reduce the plasma number density of the plasma layer, an electromagnetic $E \times B$ layer approach is proposed. The proposed $E \times B$ layer is analyzed by a two-dimensional model. It suggests that an $E \times B$ layer can be used to allow transmission of the communication signals through the plasma layer. We also propose an alternative to reduce the plasma density, based on an electrostatic plasma sheath.

Nomenclature

B = magnetic field, T
c = speed of light, m/s
E = electric field, V/m
e = electron charge, C
f_e = plasma frequency, Hz
f_w = radio wave frequency, Hz
j = current density, A/m^2
k = Boltzmann constant, 1.38×10^{-23} J/K
m = mass, kg
n = plasma number density, m^{-3}
n_e = electron number density, m^{-3}
n_i = ion number density, m^{-3}
P = pressure, N/m^2
s = sheath thickness, m
T = temperature, eV
U = voltage across the sheath, V
V = velocity, m/s
Z_i = ion mean charge number
β_e = Hall parameter
ε_0 = permittivity of vacuum, 8.5419×10^{-12} F/m
κ = signal attenuation factor, dB/m
μ = refractive index
ν_c = ion collision frequency, s^{-1}
ν_e = electron collision frequency, s^{-1}
ν_{ie} = ion-electron collision frequency, s^{-1}
ν_{in} = ion-neutral collision frequency, s^{-1}
ν_{ei} = electron-ion collision frequency, s^{-1}
ν_{en} = electron-neutral collision frequency, s^{-1}
σ = conductivity, S/m
φ = plasma potential, V
ω_e = electron Larmor frequency, rad/s
ω_{radio} = radio wave frequency, rad/s

Subscripts

e = electron
i = ion
n = neutral
0 = initial value

Presented as Paper 1394 at the 46th AIAA Aerospace Sciences Meeting and Exhibit, Reno, NV, 7–10 January 2008; received 3 March 2008; revision received 23 June 2008; accepted for publication 1 July 2008.

*Graduate Student, Department of Aerospace Engineering; minkwan@umich.edu. Student Member AIAA.

†Assistant Professor of Engineering and Applied Science, Department of Mechanical and Aerospace Engineering; keidar@gwu.edu. Senior Member AIAA.

‡Professor, Department of Aerospace Engineering; iainboyd@umich.edu. Associate Fellow AIAA.

I. Introduction

HYPERSONIC reentry and cruise vehicles, which can travel anywhere in the world within a few hours, experience communication difficulty during reentry or hypersonic flight. This difficulty is known as a communication, or radio, blackout. The cause of the blackout problem is the plasma layer, created by ionization due to the shock wave around the vehicle. When radio blackout happens, radio waves are reflected or attenuated against the plasma layer [1]. The radio waves emitted from the vehicle cannot reach a ground station or a Global Positioning System (GPS) satellite or radio waves sent to the vehicle do not reach it, and so the vehicle loses voice communication, data telemetry, GPS navigation, and electric countermeasures capability during radio blackout. Radio blackout blocks communications of the vehicle for several minutes, depending on the angle of reentry and the properties of the atmosphere [2]. For example, the Soyuz TMA (Transport Modified Anthropometric) reentry vehicle experiences about 10 min of radio blackout. Radio blackout also happens whenever the vehicle enters a planetary atmosphere at hypersonic velocity. For instance, the Mars Pathfinder experienced a 30 s radio blackout during the Mars entry mission [2].

The blackout problem is an important issue for hypersonic reentry and cruise vehicles, both for flight safety and catastrophe analysis [3]. It is very obvious that the radio blackout problem is critical for flight safety of vehicles. The radio blackout happens when the vehicle flies at hypersonic velocity. Because the vehicle losses communication with ground stations or GPS satellites, it can travel hundreds of miles during a few minutes of blackout without any GPS navigation and voice communication. In addition, the blackout makes catastrophe analysis impossible, eliminating a critical factor for understanding and preventing reentry accidents. In the Space Shuttle Colombia disaster, telemetry was lost before disintegration due to radio blackout. When the telemetry recovered from the radio blackout, there were little available data at the ground station to assist in finding the cause of the disaster. Therefore, it is extremely important to develop strategies for propagating telemetry through a plasma layer.

During the last 40 years, little progress has been made toward solving communication blackout in a reliable and acceptable manner. Most approaches for solving the radio blackout are based on altering the shape of the leading-edge geometries using a high radio wave frequency or using a magnetic field. However, all those approaches create disadvantages for aerodynamic performance, implementation costs, or system weight [4,5]. Alternative solutions have recently been proposed [5]. One of these solutions suggests communication through plasma via a Raman (3-wave) scattering process [5]. This method works well in a laboratory experiment, but it is not applicable to actual plasma layers, due to limitations such as collisional damping, sensitivity to plasma parameter nonuniformities, and a very short range of resonance for 3-wave interactions. Therefore, there is a need to develop a mitigation scheme for communication through the plasma layer that is reliable and effective. Consequently, it is extremely important to clearly understand radio blackout conditions to develop a mitigation scheme for reentry telemetry.

When a vehicle reenters or flies through the atmosphere with hypersonic velocities, it creates a shock in front of the vehicle. The created shock heats and compresses the surrounding gas so that air molecules become dissociated and ionized. This weakly ionized air creates a plasma layer around the vehicle. The created plasma layer usually has an electron number density of 10^{15} to 10^{19} m^{-3}, high enough to cause the blackout [4]. When the plasma frequency around the vehicle exceeds the radio wave frequency f_w being used to communicate between a ground station or a satellite and the vehicle, any radio wave signals are attenuated or reflected, and so the communications emitted from/to the vehicle cannot reach a ground station or vehicle. This is exactly what happens during the radio blackout. Therefore, the electron number density is important, because the plasma frequency is related to the electron number density of the plasma layer around the vehicle as follows:

$$f_e = \frac{\omega_e}{2\pi} = \frac{1}{2\pi}\sqrt{\frac{e^2 n_e}{\varepsilon_0 m_e}} \approx 8.7987 \cdot n_e^{1/2} \text{ Hz} \tag{1}$$

where n_e is the plasma density in m^{-3}. Therefore, plasma density control is important to address the radio blackout problem.

Previously, we proposed an electromagnetic $E \times B$ layer to control the plasma density and showed that it could be a strategy for propagating telemetry through a plasma layer [4,5]. The concept of the $E \times B$ layer is very simple and reliable. When an $E \times B$ layer is applied near the antenna, the plasma will be accelerated past the antenna and the number density of the accelerated plasma will decrease to satisfy mass conservation. The reduced plasma density can create a "window" in the reentry plasma layer through which radio waves can be transmitted. During the process of creating the window, the plasma density distribution will be affected by the magnitudes and profiles of the magnetic and electric fields. Numerical simulations can help to estimate this effect and determine the optimal $E \times B$ layer configuration for creating the strongest plasma number density reduction in the plasma layer.

In this paper, a two-dimensional modeling approach is applied to analyze the plasma density reduction in the $E \times B$ layer. The two-dimensional analysis demonstrates how far from the vehicle body surface the $E \times B$ layer can effectively reduce the plasma number density. This will be seen as an effective approach to solving the blackout problem. An alternative method, using an electrostatic sheath to generate a window for communication, is also suggested.

The paper is organized as follows: In Sec. II, we describe signal attenuation in terms of plasma number density and determine the required density reduction required to solve the radio blackout. The plasma density reductions in an applied $E \times B$ layer are analyzed, using the two-dimensional approach, in Sec. III. In Sec. IV, an electrostatic mitigation scheme is described as an alternative solution method.

II. Signal Attenuation

Radio wave signals experience attenuation in the plasma layer of a vehicle. The radio wave attenuation during the radio blackout is high enough to break the communication between the ground station and the vehicle. In this case, the radio wave attenuation is mainly determined by the plasma frequency f_e, which is related to the plasma number density. When the plasma frequency becomes higher than the radio wave frequency, the radio wave signal suffers infinite signal attenuation. Therefore, the plasma frequency should be less than the radio wave frequency that is used in the communication to transmit the radio wave signal. This fact limits the maximum plasma density. Table 1 shows commonly used radio wave frequencies and the corresponding limits for the maximum plasma number density for the communication through the plasma layer. At this point, the plasma density should be less than at least the maximum plasma density limit to solve the radio blackout problem.

However, there is a need to reduce the plasma density of the plasma layer below the limit based on the radio wave frequency. The plasma layer may attenuate the radio wave even when the plasma number density is lower than the limit based on the radio wave frequency. In this case, the radio wave attenuation can be expressed in terms of the plasma number density of the plasma layer. For a plasma with collision frequency ν, the radio wave attenuation can be expressed as [8]

$$\kappa = 8.69 \frac{e^2}{2\varepsilon_0 m_e c} \frac{1}{\mu} \frac{n\nu}{\omega_{\text{radio}}^2 + \nu^2} \text{ dB/m} \tag{2}$$

where n is the plasma number density, ω_{radio} is the radio wave frequency that is used for the communication, ν is the plasma collision frequency, and μ is the refractive index. The refractive index is shown at Fig. 1 in terms of the plasma angular frequency ω_e and the collision frequency ν. The collision frequency ν can be assumed to be proportional to the plasma density under typical conditions of reentry flight.

Table 1 Commonly used radio wave frequencies and their limits for the maximum plasma density [6,7]

Band name	Frequency	Plasma density limit, m^{-3}	Example uses
VHF	30–300 MHz	1.2×10^{13}–1.2×10^{15}	Aviation communication
UHF	300–3000 MHz	1.2×10^{15}–1.2×10^{17}	GPS
L band	1–2 GHz	1.3×10^{16}–5.1×10^{16}	Military telemetry
X band	8–12 GHz	8.3×10^{17}–1.9×10^{18}	Satellite communication
K_a band	27–40 GHz	9.4×10^{18}–2.1×10^{19}	Radar and experimental communication

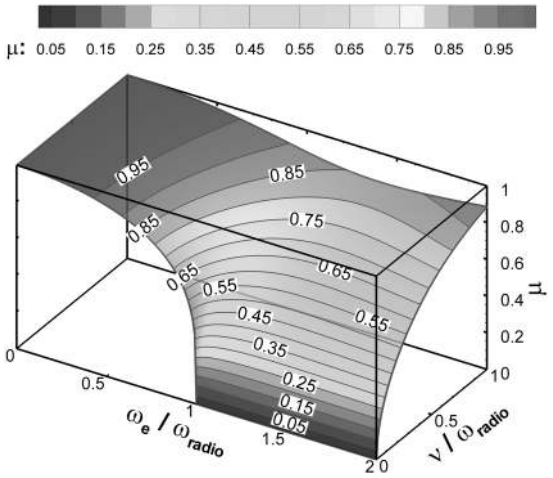

Fig. 1 Refraction index variation with plasma frequency and collision frequency.

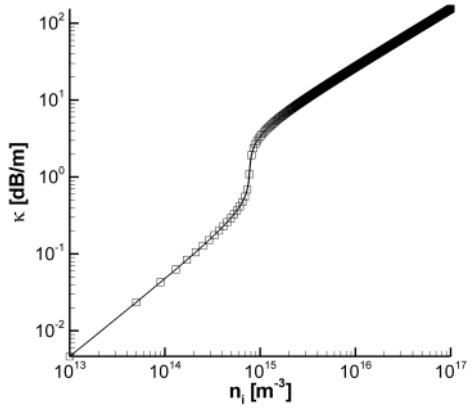

Fig. 2 Radio wave attenuation for various plasma number densities. The radio wave frequency is 1.57 GHz; a neutral number density of 10^{20} m^{-3} is used.

Consequently, the signal attenuation mainly depends on the plasma number density, because both the plasma frequency and the collision frequency are related to the plasma number density. Figure 2 shows the radio wave attenuation at the 1.57 GHz frequency generally used in GPS navigation. It shows that the radio wave attenuation decreases as the plasma number density decreases. To mitigate the radio wave attenuation, it is necessary to reduce the plasma number density. Therefore, reducing the plasma number density can be one possibility for solving the radio blackout problem.

III. Two-Dimensional Model of an $E \times B$ Layer

The previous one-dimensional approach estimates the reduced plasma density ratio for both the plasma-optic and magneto-hydrodynamic regimes [4,5]. However, the one-dimensional approach cannot determine the size of the effectively reduced plasma density region, due to the electric field. This is very important for a practical application, because the created plasma window should be larger than the size of the communication antenna. The effectively reduced plasma density area also must extend far enough from the surface to affect the plasma density peak. For example, the plasma density peak occurs at 1–2 cm above the vehicle surface in the RAM-C flight test [9,10]. To determine how far the electric field can affect the plasma, it is necessary to use a two-dimensional approach for analysis of the applied $E \times B$ layer. The applied $E \times B$ layer is shown schematically in Fig. 3. In the applied $E \times B$ layer, the electric field is created by two electrodes, and a permanent magnet provides the magnetic field. As shown in the schematics of the top view, ions are accelerated in the x and y directions. The x-direction acceleration is due to the applied electric field and the y-direction acceleration is caused by the $E \times B$ drift.

A. Mathematical Model Formulation

To simulate an $E \times B$ layer, we use a two-dimensional steady-state fluid model. It has the following general assumptions:

1) The $E \times B$ layer is quasi-neutral.
2) The neutrals are at rest.
3) There is no ionization in the $E \times B$ layer.
4) The electron temperature T_e is constant.
5) The ions are cold.
6) The magnetic field has only a z-direction component.

The stationary neutral assumption maximizes the effect of the ion-neutral drag term. The assumption of no ionization in the $E \times B$ layer is based on the fact that ionization rate is proportional to the plasma density. Because plasma density decreases in the $E \times B$ layer due to acceleration, the maximum ionization rate corresponds to unperturbed conditions [5]. Because of the cold-ion assumption, the ion-pressure term of the ion-momentum equation is negligible. Therefore, the two-dimensional steady-state $E \times B$ layer model can be described by

$$\nabla \cdot (\mathbf{V}_i n) = 0 \tag{3}$$

$$m_i n(\mathbf{V}_i \cdot \nabla \mathbf{V}_i) = en(\mathbf{E} + \mathbf{V}_i \times \mathbf{B}) - m_i n \nu_c \mathbf{V}_i \tag{4}$$

$$0 = -en(\mathbf{E} + \mathbf{V}_e \times \mathbf{B}) - kT_e \nabla n - m_e n \nu_e (\mathbf{V}_e - \mathbf{V}_i) \tag{5}$$

Because the current density is a vector in the two-dimensional case, we need to consider the current density conservation:

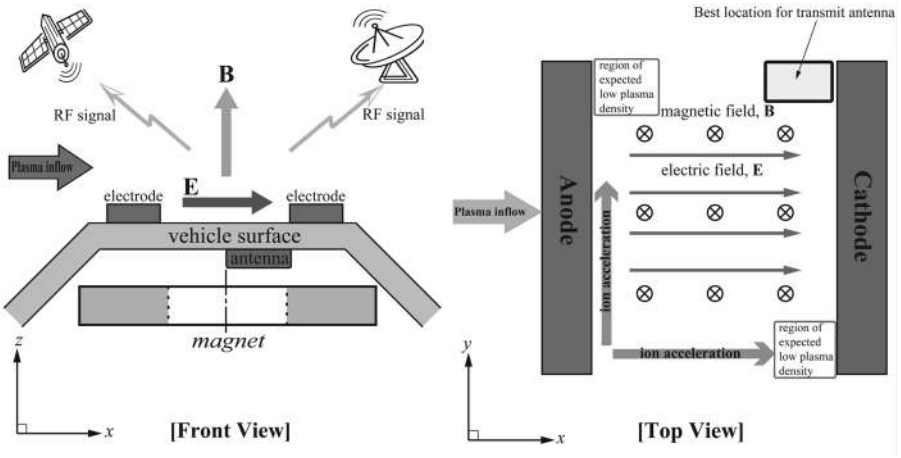

Fig. 3 Schematic of the applied electromagnetic $E \times B$ layer with two different views.

$$\nabla \cdot \mathbf{j} = 0 \tag{6}$$

The current density conservation equation (6) can be used to calculate the potential distribution under the known magnetic field distribution. In this case, the current density can be calculated from the generalized Ohm's law, which includes the Hall effect:

$$\mathbf{j} = \sigma\left(\mathbf{E} + \frac{kT_e}{e}\nabla \ell_n n - \frac{\mathbf{j}\times\mathbf{B}}{en} + (\mathbf{V}_i \times \mathbf{B})\right) \tag{7}$$

The $E \times B$ drift is in the y direction because we assume that the applied magnetic field has only a z-direction component $B = B_z$ in this work. The $E \times B$ drift does not generate any current so that the y-direction current density j_y is negligible. This occurs because electron and ion gyro radii are sufficiently small compared with the geometrical scale of the device. Then Eq. (7) may be written in component form in rectangular coordinates as follows:

$$j_x = \sigma\left(E_x + \frac{kT_e}{e}\frac{\partial \ell_n n}{\partial x} - V_y B_z\right) \tag{8}$$

$$j_z = \sigma\left(E_z + \frac{kT_e}{e}\frac{\partial \ell_n n}{\partial z}\right) \tag{9}$$

where σ is the electron conductivity, E_x and E_z are the x-direction and z-direction components of the electric field, and j_x and j_z are the x-direction and z-direction components of the current density, respectively. In this case, we can use a drift velocity in the $E \times B$ direction as

$$V_y = -V_x\frac{\omega_e}{\nu_e} = -V_x\beta_e \tag{10}$$

where ω_e is the electron cyclotron frequency and β_e is the Hall parameter.

Equations (6), (8), and (9) can be used to express the equation for the electric field in an explicit form. Because the Coulomb logarithm is only weakly dependent on the plasma number density n, the electron collision frequency is proportional to the plasma number density as follows:

$$\nu_{\text{ei}} = \text{constant} \cdot n \tag{11}$$

Using Eqs. (6) and (8–11), the following expression is obtained for the potential distribution φ:

$$\begin{aligned}&\frac{1}{1+\beta_e^2}\frac{\partial^2\phi}{\partial x^2} + \frac{\partial^2\phi}{\partial z^2} + \left(\frac{2\beta_e^2}{(1+\beta_e^2)^2}\frac{\partial \ell_n n}{\partial x}\right)\frac{\partial\phi}{\partial x} - T_e\frac{1}{n}\frac{\partial^2 n}{\partial z^2}\\ &+ T_e\left(\frac{\partial \ell_n n}{\partial z}\right)^2 - \frac{2\beta_e^2}{(1+\beta_e^2)^2}T_e\left(\frac{\partial \ell_n n}{\partial x}\right)^2 - \frac{T_e}{1+\beta_e^2}\frac{1}{n}\frac{\partial^2 n}{\partial z^2}\\ &+ \frac{T_e}{1+\beta_e^2}\left(\frac{\partial \ell_n n}{\partial x}\right)^2 = 0\end{aligned} \tag{12}$$

Equation (12) describes the potential distribution of the two-dimensional approach in a form similar to a Poisson equation, which is obtained for the current density conservation. The system of equations (3), (4), and (12) describe the mathematical model of the two-dimensional approach.

B. Numerical Method and Boundary Conditions

The two-dimensional $E \times B$ layer model is solved numerically with an iterative scheme. Initially, it begins with assuming the initial potential distribution ϕ^0. The initial guess of the potential is obtained by solving the Poisson equation. The estimated potential distribution is differentiated to give the electric field. The calculated electric field is used to solve the ion transport equations (3) and (4). The ion transport equation is solved by using the finite volume method with the Harten–Lax–van Leer contact wave solver [11,12] and gives plasma number density and velocity. The obtained plasma number density and velocity distribution are used as coefficients in the potential distribution equation (12). The potential distribution equation is solved by the alternating-direction implicit method [13,14], and we can obtain the new potential distribution for the next iteration. After several iterations, the potential distribution converges and we obtain a steady-state solution with sufficient accuracy.

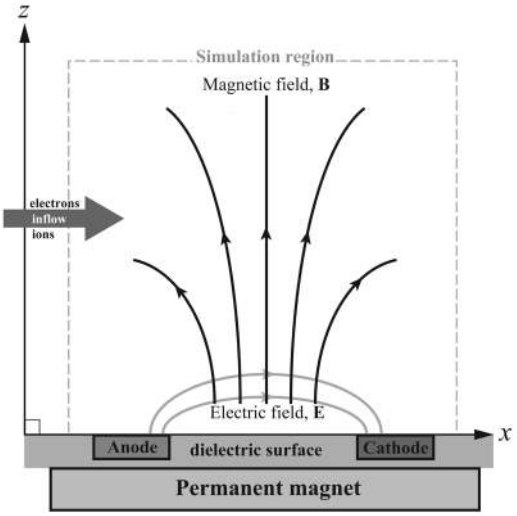

Fig. 4 Schematic of the $E \times B$ layer for the two-dimensional approach. In this approach, we assume that the magnetic field is constant and it has only a z-direction component.

The schematic diagram of the two-dimensional simulation domain is shown in Fig. 4. In this work, we will simulate the x–z plane. In the simulated domain, the inflow boundary condition is applied for the left side. It uses the initial plasma number density and the constant neutral number density. In this case, the bulk plasma velocity is assumed to be 1000 m/s and has only an x-direction component. The right and upper side boundaries of Fig. 4 use the outflow boundary condition, and no potential variation across the boundary is assumed. The bottom boundary of Fig. 4 uses the dielectric boundary condition, because the suggested $E \times B$ layer used a dielectric material on the bottom surface. Because of the dielectric boundary condition, no ions are neutralized at the dielectric wall, which means that the wall fully absorbs ions.

C. Results

The plasma density reduction is the plasma density normalized by the plasma bulk density n_0. A small plasma density reduction indicates a weak effect of the applied $E \times B$ layer. A large plasma density reduction indicates a strong effect of the applied $E \times B$ layer.

The calculated plasma density reduction is shown in Fig. 5. It shows the plasma density reduction distribution in the x–z plane when the $E \times B$ layer is applied. The applied $E \times B$ layer has a -100 V potential drop between the anode and the cathode. The anode and cathode are 5 mm in length and are located at $x = 0$ and 10 cm, respectively. The $E \times B$ layer has a constant one-dimensional magnetic field along the negative z direction and it has 0.1 T strength. In this study, we use a plasma of nitrogen with a constant background neutral density of 10^{20} m^{-3} (which corresponds to a pressure of about 3 mtorr) and 10^{18} m^{-3} bulk plasma number density with 1000 m/s bulk velocity.

The plasma density reduction distribution shows the location of the lowest plasma number density in the applied $E \times B$ layer that provides the optimal location for the antenna, which is indicated in Fig. 5. It also shows how far the electric field can affect the plasma. The effects of plasma density reduction decrease with distance from the wall, as one can see in Fig. 5. The plasma density reduction distributions along the z direction are shown in Fig. 6. As shown in Figs. 5 and 6, the plasma density reductions of the applied $E \times B$ layer become ineffective at 4 cm from the bottom dielectric wall. These are very promising results for mitigating the radio blackout problem, because the plasma density peak in the RAM-C flight is at about 1–2 cm from the vehicle surface [5].

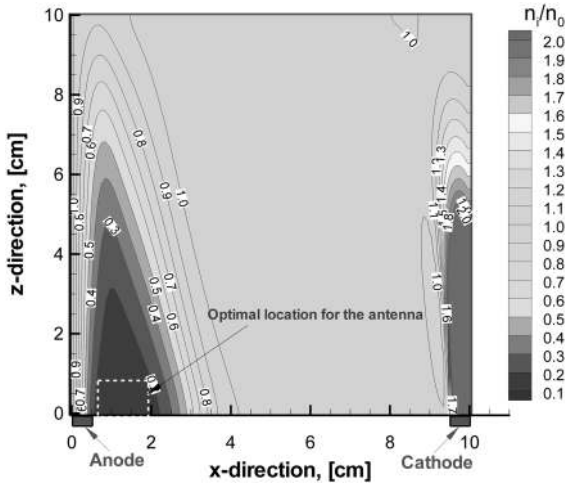

Fig. 5 Plasma number density reduction distribution in the applied $E \times B$ layer. The bulk plasma density is 10^{18} m^{-3} and velocity is 1000 m/s. The background neutral number density is 10^{20} m^{-3}.

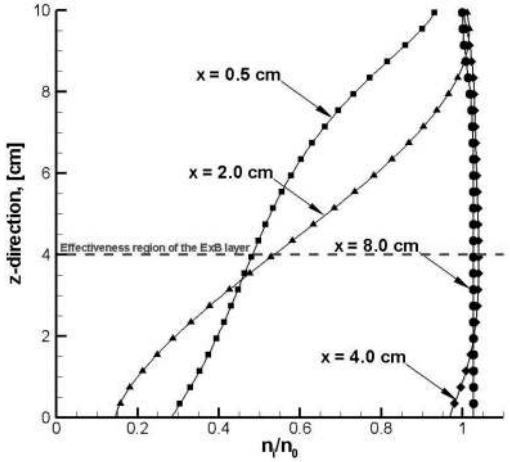

Fig. 6 Plasma number density reduction along the z direction at several x locations.

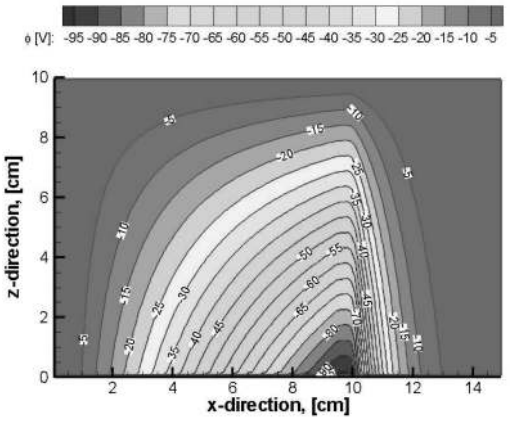

Fig. 7 Distribution of the potential of the applied $E \times B$ layer with 0.1 T magnetic field. The applied potential drop between the anode and the cathode is −100 V.

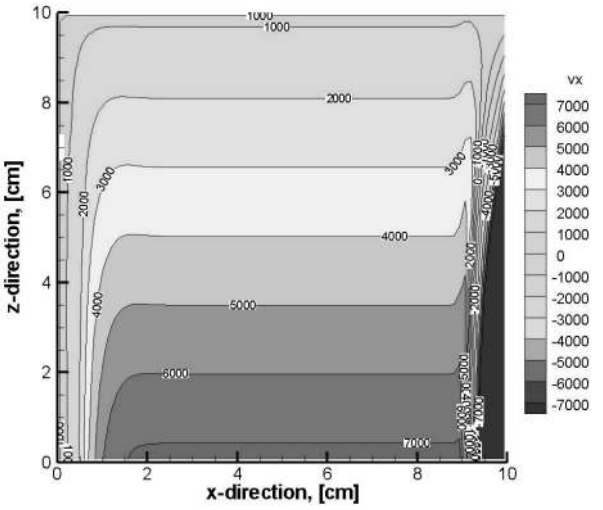

Fig. 8 Distribution of ion velocities in the x direction. The bulk plasma velocity is 1000 m/s.

The plasma number density distribution of Fig. 5 shows some increased density near the cathode. This is caused by the potential distribution. The potential distribution in the applied $E \times B$ layer is shown in Fig. 7. It shows that the potential sharply drops just beyond the cathode. This is primarily caused by the 0 V potential beyond the cathode. The applied 0 V potential is quite reasonable, because we assume that the area beyond the cathode has a vacuum condition. The sharp drop potential of this area creates a large negative electric field along the x direction. Because of the negative electric field, the ions are decelerated in this direction. The decelerated ions create negative ion flow near the cathode. The negative ion flow is seen in Fig. 8, which shows the ion velocity of the x-direction component. As one can see, the ion flow changes direction at the front of the cathode so that the ions stagnate near the cathode. Consequently, the stagnated ions explain the increased ion number density near the cathode. This fact is very important in deciding the optimal location of the transmission.

IV. Alternative Method: Electrostatic Sheath

As an alternative method to mitigate the blackout problem, we consider an electrostatic plasma sheath [5,15]. An electrostatic plasma sheath is formed when a negative voltage is applied to a cathode in a plasma. In the electrostatic plasma sheath, the electrons are depleted due to the applied negative voltage. The depleted electron region may provide a possible way to communicate through the plasma layer. This is possible because there are almost no electrons in the electrostatic plasma sheath to interfere with electromagnetic waves [5]. Thus, the electrostatic plasma sheath can provide a window for communication during the radio blackout. In this case, the size of the electrostatic plasma sheath is important because it must contain the physical size of the transmission and/or reception antennas. In this section, we consider two different types of electrodes: a U-shaped electrode and a cylindrically shaped electrode. The two electrodes are shown schematically in Fig. 9.

In the one-dimensional steady-state case, the sheath thickness can be estimated according to the Child–Langmuir law [5,16–18] as

$$s = \left(\frac{4}{9}\varepsilon_0\right)^{1/2}\left(\frac{2Z_i e}{m_i}\right)^{1/4}\frac{\Delta\phi^{3/4}}{(eZ_i n V_i)^{1/2}} \tag{13}$$

However, it is difficult to use the Child–Langmuir law for the two-dimensional steady-state case, because the Child–Langmuir law is only valid for a one-dimensional, or plate, electrode. To simulate the two-dimensional electrostatic sheath, we employ a steady-state two-dimensional fluid-sheath model that is based on the time-dependent fluid-sheath model [15,19,20]. It makes two main assumptions to model the collisional sheath [21]. First, it assumes that the sheath has a uniform background neutral density and the ions are cold. The uniform background neutral density introduces collision drag terms into the two-dimensional fluid-sheath model. Because of the cold-ion assumption, the ion-pressure term of the ion-momentum equation is negligible. Second, it assumes that the electrons satisfy the Boltzmann relation in the sheath model, which can be coupled with

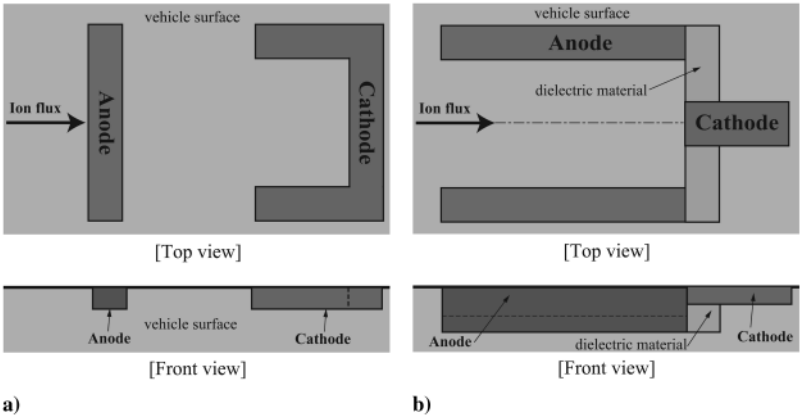

Fig. 9 Schematics of the two different types of electrodes as an alternative method to solve the radio blackout problem: a) U-shaped electrode and b) cylindrically shaped electrode.

Poisson's equation for the electric potential. Therefore, the steady-state two-dimensional collisional sheath can be described by

$$\nabla \cdot (n_i \mathbf{u}_i) = 0 \tag{14}$$

$$m_i \nabla \cdot (n_i \mathbf{u}_i \mathbf{u}_i) = e n_i \mathbf{E} - \nu_c m_i n_i \mathbf{u}_i \tag{15}$$

$$n_e = n_0 \exp(e\phi / kT_e) \tag{16}$$

$$\nabla^2 \phi = -e/\varepsilon_0 (n_i - n_e) \tag{17}$$

Equations (14–17) are solved numerically with an iterative scheme. The ion number densities and velocities are calculated by using a similar method to the $E \times B$ layer simulation. In this case, the plasma is not quasi-neutral, and so we need to calculate the electron density using the Boltzmann relation [Eq. (16)]. The calculated electron and ion number densities give a new potential distribution that is calculated by solving Poisson's equation (17). The calculated new potential distribution gives a new electric field for the next iteration step. After a sufficient number of iterations, we can obtain a steady-state solution with sufficient accuracy.

A −1000 V potential drop, applied across the two electrodes, is large compared with the electron temperature, which is assumed as 1.5 eV. In this work, we use a plasma of molecular nitrogen with 10^{20} m^{-3} neutral background density, which corresponds to 3 mtorr pressure condition. In the collisional electrostatic-plasma-sheath regime, the initial ion flow velocity is not known, but the physical limits of it will be at or below the Bohm velocity [22–24]. This classical condition for the sheath formation is applicable for our electrostatic-sheath cases. Because we consider formation of the electrostatic layer in the boundary layer of the hypersonic flowfield, the velocity of the boundary layer is small and typically smaller than the Bohm velocity. Thus, we use 1000 m/s as the initial ion flow velocity and the bulk electron number density is 10^{18} m^{-3}. Parameters of the undisturbed plasma correspond to a hypersonic flowfield calculated using a particle simulation technique [5].

The calculated results are shown in Figs. 10 and 11. They show the calculated distributions of the electron number density, which are normalized by the bulk electron density n_0, and the potential near the two types of electrodes. The electron number density distribution shows the depleted region: the sheath. The sheath region of Fig. 10 extends approximately 4 cm over the dielectric surface material. This may satisfy the requirement of affecting the plasma density peak with a standoff distance of several centimeters [4]. On the other hand, the size of the electrostatic sheath also can be estimated from Figs. 10 and 11. Figure 10 shows that the U-shaped electrode can create a sheath thickness of about 3 cm. Using the same conditions as those employed for the U-shaped electrode, Eq. (13) gives a one-dimensional sheath thickness of 1.67 cm that is almost a factor of 2 smaller than the result from the two-dimensional simulation. Figure 11 shows that the cylindrically shaped electrodes give a

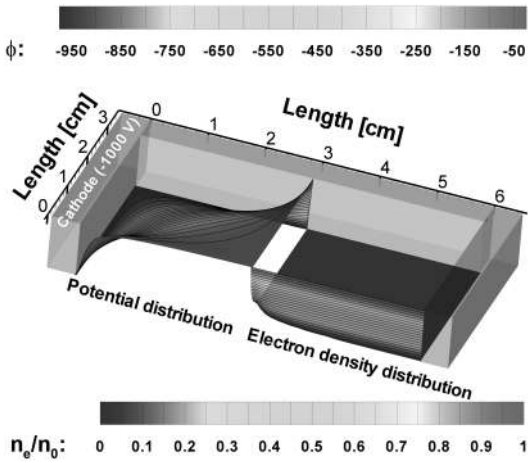

Fig. 10 Potential and electron number density distributions of the U-shaped electrode including a schematic of the electrodes. The bulk plasma density n_0 is 10^{18} m^{-3}, and the neutral background density n_n is 10^{20} m^{-3}. The cathode is at −1000 V potential.

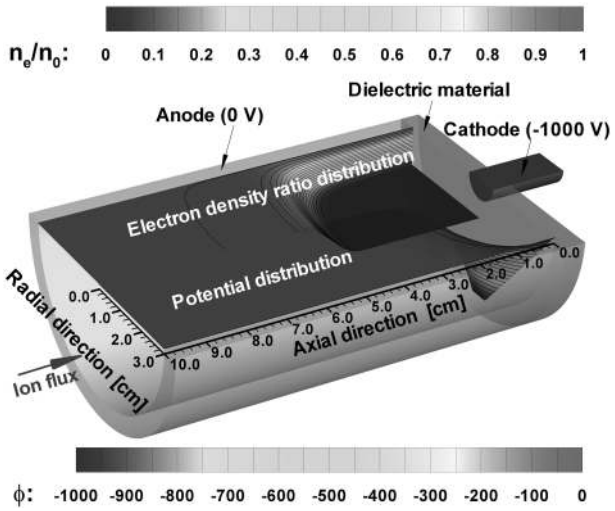

Fig. 11 Potential and electron number density distributions of the cylindrically shaped electrodes including a schematic of the electrodes. The bulk plasma density n_0 is 10^{18} m^{-3} and the neutral background density n_n is 10^{20} m^{-3}. The cathode is at −1000 V potential.

sheath having a radius of about 1.0 cm at the 4.0 cm axial position. The size of the electrostatic sheath will be maximized when an $E \times B$ layer is applied, because the applied $E \times B$ layer decreases the bulk electron number density. When the size of the electrostatic sheath becomes comparable to the size of the transmission antenna, it may allow transmission through the plasma layer during the radio blackout.

V. Conclusions

We proposed the $E \times B$ layer configuration to be necessary to allow communication through the plasma layer during the radio blackout period. In this case, the effective area of the applied $E \times B$ layer is important, because it must be larger than the size of the antenna and greater than the distance of the peak plasma density in the plasma layer from the vehicle surface. The effectiveness area of the applied $E \times B$ layer is simulated by a two-dimensional approach. It is shown that the applied $E \times B$ layer can effectively reduce the plasma number density approximately 3 cm from the dielectric wall. We also investigate the two-dimensional shaped electrodes. The two-dimensional shaped electrodes create an electron-depleted region, the sheath, and it can be another mitigation scheme for the reentry telemetry. Consequently, the possibility of communication during the radio blackout will be maximized by a combination of an $E \times B$ layer and a two-dimensional shaped electrode.

Acknowledgments

The authors gratefully acknowledge the support of the U.S. Air Force in funding this work, through the Phase-II Small Business Innovation Research grant titled "ReComm-ReEntry and Hypersonic Vehicle Plasma Communications System," contract FA8718-06-C-0038. The authors wish to thank David Morris, Chris Davis, Joseph Mancuso, Kristina Lemmer, Jonathan Zagel, and John Yim for very useful discussions on this subject.

References

[1] Rybak, J., and Churchill, R., "Progress in Reentry Communications," *IEEE Transactions on Aerospace and Electronic Systems*, Vol. aes-7, No. 5, Sept. 1971, pp. 879–894. doi:10.1109/TAES.1971.310328

[2] Roers, L., "Communications–Blackout," *It's ONLY Rocket Science*, Astronomers' Universe Series, Springer, New York, 2008, pp. 158–161.

[3] Starkey, R., Lewis, R., and Jones, C., "Plasma Telemetry in Hypersonic Flight," International Telemetering Conference, San Diego, CA, International Foundation for Telemetering Paper 02-15-2, 2002.

[4] Kim, M., Keidar, M., Boyd, I. D., and Morris, D., "Plasma Density Reduction Using Electromagnetic $E \times B$ Field During Reentry Flight," International Telemetering Conference, Las Vegas, NV, International Foundation for Telemetering Paper 07-19-03, Oct. 2007.

[5] Keidar, M., Kim, M., and Boyd, I. D., "Electromagnetic Reduction of Plasma Density During Atmospheric Reentry and Hypersonic Flights," *Journal of Spacecraft and Rockets*, Vol. 45, No. 3, 2008, pp. 445–453. doi:10.2514/1.32147

[6] *Manual of Regulations and Procedures for Federal Radio Frequency Management*, May 2003 ed., Jan. 2007 rev., National Telecommunications and Information Administration, Washington, D.C., 2007, Chap. 4.

[7] *United States Frequency Allocations: The Radio Spectrum*, National Telecommunications and Information Administration, Washington, D.C., Oct. 2003.

[8] Christopher, P., "Millimeter-Wave Communications for Atmospheric Reentry Vehicles," *Proceedings of SPIE*, Vol. 3232, 1998, pp. 21–32. doi:10.1117/12.301031

[9] Scalabrin, L. C. and Boyd, I. D., "Numerical Simulation of Weakly Ionized Hypersonic Flow for Reentry Configurations," AIAA Paper 2006-3773, June 2006.

[10] Park, C., *Nonequilibrium Hypersonic Aerodynamics*, Wiley, New York, 1990, Chap. 8.

[11] Colella, P., Dorr, M. R., and Wake, D. D., "A Conservative Finite Difference Method for the Numerical Solution of Plasma Fluid Equations," Journal of Computational Physics, Vol. 149, No. 1, 1999, pp. 168–193.

[12] Li, S., "An HLLC Riemann Solver for Magneto-Hydrodynamics," *Journal of Computational Physics*, Vol. 203, No. 1, 2005, pp. 344–357. doi:10.1016/j.jcp.2004.08.020

[13] Keidar, M., Beilis, I. I., Boxman, R. L., and Goldsmith, S., "2D Expansion of the Low-Density Interelectrode Vacuum Arc Plasma Jet in an Axial Magnetic Field," *Journal of Physics D: Applied Physics*, Vol. 29, No. 7, 1996, pp. 1973–1983. doi:10.1088/0022-3727/29/7/034

[14] Tannehill, J. C., Anderson, D. A., and Pletcher, R. H., *Computational Fluid Mechanics and Heat Transfer*, 2nd ed., Taylor and Francis, Washington, D.C., 1997, Chap. 4.

[15] Kim, M., Keidar, M., and Boyd, I. D., "Electrostatic Manipulation of a Hypersonic Plasma Layer: Images of the 2D Sheath," *IEEE Transactions on Plasma Science*, Vol. 36, No. 4, 2008, pp. 1198–1199. doi:10.1109/TPS.2008.926968

[16] Child, C. D., "Discharge from Hot CaO," *Physical Review (Series I)*, Vol. 32, No. 5, 1911, pp. 492–511.10.1103/PhysRevSeriesI.32.492

[17] Langmuir, I., "The Effect of Space Charge and Residual Gases on Thermionic Currents in High Vacuum," *Physical Review (Series II)*, Vol. 2, No. 6, 1913, pp. 450–486.10.1103/PhysRev.2.450

[18] Keidar, M., Boyd, I. D., and Beilis, I. I., "Modeling of a High-Power Thruster with Anode Layer," *Physics of Plasmas*, Vol. 11, No. 4, Apr. 2004, pp. 1715–1722. doi:10.1063/1.1668642

[19] Kim, D., and Economou, D. J., "Simulation of a Two-Dimensional Sheath over a Flat Wall with an Insulator/Conductor Interface Exposed to a High Density Plasma," *Journal of Applied Physics*, Vol. 94, No. 5, Sept. 2003, pp. 2852–2857. doi:10.1063/1.1597943

[20] Hong, M., and Emmert, G. A., "Two-Dimensional Fluid Modeling of Time-Dependent Plasma Sheath," *Journal of Vacuum Science and Technology B (Microelectronics and Nanometer Structures)*, Vol. 12, No. 2, 1994, pp. 889–896. doi:10.1116/1.587322

[21] Porwitzky, A. J., Keidar, M., and Boyd, I. D., "On the Mechanism of Energy Transfer in the Plasma-Propellant Interaction," *Propellants, Explosives, Pyrotechnics*, Vol. 32, No. 5, 2007, pp. 385–391. doi:10.1002/prep.200700042

[22] Franklin, R. N., "What Significance Does the Bohm Criterion has in an Active Collisional Plasma-Sheath?," *Journal of Physics D: Applied Physics*, Vol. 35, No. 18, 2002, pp. 2270–2273. doi:10.1088/0022-3727/35/18/307

[23] Leibermann, M. A., and Lichtenberg, A. J., "Bohm Sheath Criterion," *Principles of Plasma Discharges and Materials Processing*, 2nd ed., Wiley, New York, 2005, pp. 168–175.

[24] Keidar, M., Boyd, I. D., and Beilis, I. I., "Plasma Flow and Plasma-Wall Transition in Hall Thruster Channel," *Physics of Plasmas*, Vol. 8, No. 12, 2001, pp. 5315–5322. doi:10.1063/1.1421370

A. Ketsdever
Associate Editor